Journal of Cellular Physiology

TNF-α Upregulates Sclerostin Expression in Obese Mice Fed a High-Fat Diet

KYUNGHWA BAEK,[1,2] HYO RIN HWANG,[1] HYUN-JUNG PARK,[1] ARANG KWON,[1] ABDUL S. QADIR,[1] SEONG-HEE KO,[2] KYUNG MI WOO,[1] HYUN-MO RYOO,[1] GWAN-SHIK KIM,[1] AND JEONG-HWA BAEK[1]*

[1]*Department of Molecular Genetics, School of Dentistry and Dental Research Institute, Seoul National University, Seoul, Korea*

[2]*Department of Pharmacology, College of Dentistry and Research Institute of Oral Science, Gangneung-Wonju National University, Gangwondo, Korea*

Sclerostin decreases bone mass by antagonizing the Wnt signaling pathway. We examined whether obesity-induced bone loss is associated with the expression of sclerostin. Five-week-old male mice were assigned to one of two groups (n = 10 each) and fed either a control diet (10% kcal from fat; CON) or a high-fat diet (60% kcal from fat; HF) for 12 weeks. Thex final body weight and whole body fat mass of the HF mice were higher than those of the CON mice. The distal femur cancellous bone mineral density and bone formation rate was lower in HF mice than in CON mice. The percent erosion surface was higher in the HF mice than the CON mice. The serum levels and femoral osteocytic protein expression levels of tumor necrosis factor-α (TNF-α) were significantly higher in HF mice than in CON mice. Sclerostin mRNA levels and osteocytic sclerostin protein levels in femoral cortex were also higher in HF mice than in CON mice. Sclerostin expression in MLO-Y4 osteocytes increased with TNF-α treatment, and TNF-α-induced sclerostin expression was blocked by the inhibition of NF-κB activation. Chromatin immunoprecipitation and a luciferase reporter assay demonstrated that NF-κB directly binds to the NF-κB binding elements on the mouse *sost* promoter and stimulates sclerostin expression. These results support a model in which, in the context of obesity or other inflammatory diseases that increase the production of TNF-α, TNF-α upregulates the expression of sclerostin through NF-κB signaling pathway, thus contributing to bone loss.

J. Cell. Physiol. 229: 640–650, 2014.

Obesity has been traditionally thought to benefit bone integrity because of the mechanical loading conferred by body weight. However, it has been recently demonstrated that low bone mass and high fracture risk are associated with obesity in both animals (Chen et al., 2010) and humans (Chan and Chen, 2009). Although somewhat controversial, several mechanisms have been posed to explain how accumulated body fat is detrimental to bone mass (Zhao et al., 2007, 2008; Chen et al., 2010). Obesity may increase adipocyte differentiation and fat accumulation while decreasing osteoblast differentiation and bone formation in the bone marrow (Zhao et al., 2008). A high-fat diet may interfere with intestinal calcium absorption and therefore decrease the calcium available for bone formation (Xiao et al., 2010). Additionally, the levels of adipocyte-derived adipokines are altered by body composition and may affect bone metabolism. Although controversial, leptin is a representative adipokine that links bone and energy metabolism. Centrally acting leptin binds to its receptor in the hypothalamic region and negatively regulates bone mass through a sympathetic nervous system relay (Takeda et al., 2002). Peripheral leptin, however, appears to positively regulate bone mass, especially in the context of circumstances that induce bone loss (Baek and Bloomfield, 2009; Baek and Bloomfield, 2012). Another adipokine, adiponectin, is known to improve insulin sensitivity, and the circulating levels of adiponectin are decreased in obese and diabetic subjects. Adiponectin is thought to negatively regulate bone mass and be an independent predictor of low bone mass (Bacchetta et al., 2009; Bozic et al., 2010). Because of these contradictory effects of adipokines on bone metabolism, the underlying pathophysiological mechanism between obesity and bone integrity is very complex and has not been fully investigated.

Obesity is closely linked to chronic inflammation and is characterized by increased production of inflammatory cytokines, such as tumor necrosis factor-α (TNF-α), and the activation of the inflammatory signaling network (Hotamisligil, 2006). TNF-α is a multifunctional cytokine that regulates various cellular and biological processes such as cell proliferation, differentiation, apoptosis, and immune function (Cope et al., 1997). TNF-α suppresses osteoblast differentiation and bone formation partially through NF-κB activation (McMahon and Ueki, 2008; Lee et al., 2010) and accelerates bone resorption partially by upregulating the expression of the receptor activator of NF-κB ligand (Rankl) (Zhang et al., 2001).

Sclerostin, the osteocyte-specific cysteine knot-secreted glycoprotein, is encoded by the *sost* gene. Patients with *SOST*

Conflict of interest: nothing to declare.

Contract grant sponsor: National Research Foundation of Korea (NRF-MEST);
Contract grant numbers: 2011-0016548, 2010-0005836.

*Correspondence to: Jeong-Hwa Baek, Department of Molecular Genetics, School of Dentistry, Seoul National University, 28 Yeongun-dong, Jongno-gu, Seoul 110-749, Korea.
E-mail: baekjh@snu.ac.kr

Manuscript Received: 9 July 2013
Manuscript Accepted: 3 October 2013

Accepted manuscript online in Wiley Online Library (wileyonlinelibrary.com): 8 October 2013.
DOI: 10.1002/jcp.24487

mutations and *sost*-deficient mice exhibit very high bone mass, suggesting that this molecule has a key role in the regulation of bone mass (Brunkow et al., 2001; Li et al., 2008). Canonical Wnt signaling pathway causes an accumulation of β-catenin in the cytosol and its ultimate translocation into the nucleus, where β-catenin acts as a transcriptional coactivator of transcription factors that belong to the TCF/LEF family. Wnt signaling begins when Wnt ligand binds the Frizzled family receptor, and co-receptors including lipoprotein receptor-related protein 5/6 (Lrp5/6) facilitate this ligand-receptor interaction. Sclerostin binds to Lrp5/6 and antagonizes Wnt signaling, thus lowering bone mass. Recent reports show that level of circulating sclerostin is positively associated with obesity (Urano et al., 2012). In addition, TNF-α induces the mitogen-activated protein kinase (MAPK)-dependent expression of sclerostin in human osteoblasts, indicating that sclerostin plays a role in inflammatory disease-induced bone loss (Vincent et al., 2009).

In the present study, we examined whether obesity-induced bone loss is associated with sclerostin expression. Additionally, because increased production of TNF-α has been implicated in metabolic diseases such as obesity, we investigated the molecular mechanism of TNF-α-induced sclerostin expression in the osteocyte-like cell line MLO-Y4.

Materials and Methods

Animals and experimental design

Twenty C57BL/6 mice, aged 5 weeks at purchase (Orient Bio, Seoul, Korea), were housed in individual cages on a 12:12 light:dark cycle and were fed an AIN93-M purified diet (Research Diets; New Brunswick, NJ) for 1 week before the start of the experiment. The AIN93-M diet most closely matches the National Research Council recommendations for mature rat dietary requirements (Reeves et al., 1993a,b). Mice were block assigned by body weight into two groups of ten animals each: *ad-lib* fed controls (CON) and mice fed a high-fat diet (HF). The CON group was fed a control diet (10% kcal from fat) for the 12-week protocol. For the high-fat diet (60% kcal from fat; Research Diets #D12492) experiments, mice were fed a high-fat diet from the age of 6 to 18 weeks. Food intake for the all of the mice was measured each day.

At 9 and 2 days before sacrifice, the animals were given subcutaneous injections of calcein (25 mg/kg) to label mineralizing bone for histomorphometric analysis. Immediately before sacrificing, animals were anesthetized with an injectable cocktail of ketamine and xylazine and were subjected to dual energy X-ray absorptiometry (pDEXA, Norland Stratec Medizintechnik GmbH, Birkenfeld, Germany) whole body scans. Anesthetized mice were scanned while positions prone on the platform, and their total body fat mass and lean mass were measured. All procedures in this study were approved by the Institute of Laboratory Animal Resources at Seoul National University.

Trabecular and cortical bone morphology by μCT

Assessment of bone morphology and microarchitecture was performed using high-resolution microcomputed tomography (μCT 1172, Skyscan1172, SKYSCAN, Antwerp, Belgium). In brief, the distal femoral metaphysis was scanned using an X-ray energy of 70 KeV, an integration time of 200 msec and a 12-μm isotropic voxel size. For the cancellous bone region, we assessed the trabecular bone mineral density (Tb.BMD, mg/cm^3), bone volume fraction (BV/TV, %), trabecular thickness (Tb.Th, mcm), trabecular separation (Tb.Sp, mcm), trabecular number (Tb.N, 1/mm) and connectivity density (ConnD, 1/mm^3). Transverse CT slices were also acquired at the femoral midshaft to assess the cross-sectional bone area (B.Ar, mm^2), cross-sectional diameter (CD, mcm), periosteal perimeter (T.Pm, mcm), medullar area (M.Ar, mm^2), cortical thickness (Cs.Th, mcm), and polar moment of inertia (pMOI, mm^4) (Parfitt et al., 1987; Dempster et al., 2013).

Bone histomorphometry

Undemineralized distal left femora were subjected to serial dehydration and embedded in methylmethacrylate. Serial frontal sections were cut into 8 and 4 μm slices: 8 μm sections were left unstained for calcein fluorochrome label measurements to assess kinetic measures, including mineralizing surface, mineral apposition rate and bone formation rate; 4 μm sections were treated with von Kossa/tetrachrome stain to assess static measures, including cancellous bone volume and surfaces covered by osteoblasts, osteoid matrix, and osteoclasts. Histomorphometric analyses were performed with the OsteoMeasure system (OsteoMetrics, Inc., Atlanta, GA) interfaced with a color video camera (DXC-390P, Sony, Japan) and an Olympus BX60 Microscope with epifluorescent lights (Leeds Instruments, Inc., Irving, TX). At 20x magnification, a defined region of interest encompassing 5–6 mm^2 was established approximately 1.0 mm from the growth plate and within the endocortical edges. The total bone surface, single-labeled surface, and double-labeled surface were measured at 100×, and the inter-label distances, bone volume and osteoid/osteoblast surface were measured at 200×. The mineral apposition rate (MAR, mcm/day) was calculated by dividing the average inter-label width by the time between labels (7 days), and the mineralizing surface per cancellous bone surface (MS/BS) was calculated using the formula MS/BS = {[(single labeled surface/2) + double label surface]/surface perimeter} × 100. The bone formation rate (BFR, mcm^3/mcm^2/day) was calculated as MAR × MS/BS. Total bone, osteoid and eroded surfaces were obtained by manual tracing. The derived indices of bone volume/tissue volume (BV/TV), osteoid surface/bone surface (OS/BS), eroded surface/bone surface (ES/BS), and osteoid thickness (O.Th), were calculated using previously described formulae (Baek and Bloomfield, 2012). The nomenclature for the histomorphometry follows the standard usage (Parfitt et al., 1987; Dempster et al., 2013).

Immunohistochemistry and serum TNF-α analyses

Femur specimens from mice were fixed with neutral-buffered formalin, decalcified with 10% EDTA and embedded in paraffin. Sections of the proximal femur (5 μm thick) were immunostained for sclerostin or TNF-α using an avidin–biotin technique (Hsu et al., 1981). Briefly, sections were incubated overnight at 4°C with 1:200 diluted anti-TNF-α antibody (Bioworld Technology, St. Louis Park, MN) or 1:5 diluted anti-sclerostin antibody (Santa Cruz Biotech, Dallas, TX). Sections then were incubated with the corresponding biotinylated anti-rabbit IgG secondary antibody and finally with an ABC complex (Vectastain elite ABC reagent; VECTOR, Burlingame, CA). Peroxidase activity was visualized by developing the sections with the enzyme's substrate (NovaRED substrate kit; VECTOR). The specificity of the method was tested by omitting the primary antibody in the immunostaining procedures as a negative control.

A mouse TNF-α ELISA kit (Crystal Chem, Chicago, IL) was used to measure the concentration of TNF-α in serum samples. Assays were performed on duplicate samples.

Cell culture

MLO-Y4 cells, a murine osteocyte-like cell line, were maintained in alpha modified Eagle's medium (αMEM; Hyclone, Logan, UT) supplemented with 2.5% fetal bovine serum and 2.5% calf serum (BioWhittaker, Walkersville, MD).

Reverse transcription-polymerase chain reaction (RT-PCR)

To evaluate mRNA expression, quantitative RT-PCR was performed. Total RNA was isolated from tibiae samples or MLO-

Y4 cells using an RNeasy kit (Qiagen, Valencia, CA). First-strand cDNA was synthesized from total RNA using the AccuPower RT PreMix (Bioneer, Daejeon, Korea) and was subsequently used for quantitative real time-PCR amplification using SYBR premix EX Taq (Takara, Otsu, Japan). Mouse genes and the sequences of the PCR primers used for real-time PCR are shown in Table I. Gapdh was used as the reference to normalize each sample for quantification.

Western blot analysis

The cells were washed with PBS and scraped into lysis buffer (10 mM Tris–Cl (pH 7.5), 150 mM NaCl, 1 mM EDTA (pH 8.0), 1% Triton X-100, 0.5% sodium deoxycholate, 0.1% SDS, 50 mM sodium fluoride, 0.2 mM sodium orthovanadate, 1 mM PMSF, 1 μg/ml aprotinin, 1 μM leupeptin, and 1 μM pepstatin) and sonicated briefly. Equal amounts of protein were subjected to SDS-PAGE and subsequently electro-transferred onto a PVDF membrane. The membranes were blocked for 1 h with 5% nonfat dry milk, incubated overnight at 4°C with 1:1,000 diluted anti-sclerostin antibody (Santa Cruz) or anti-NF-κB p65 antibody (Santa Cruz) and subsequently incubated with HRP-conjugated secondary antibody. Labeled protein bands were visualized using Supex reagent (Dyne-Bio, Sungnam, Korea), and luminescence was detected with a LAS1000 (Fuji Photo Film, Tokyo, Japan).

RNA interference of NF-κB

MLO-Y4 cells were transfected with siRNA using Dharmafect (Dharmacon, Lafayette, CO) according to the manufacturer's instructions. siGENOME ON-TARGETplus SMARTpool mouse NF-κB p65 siRNA (L-040776-00) and nontargeting control scrambled siRNA (D-001810-10) were purchased from Dharmacon. The efficacy of knockdown was assessed by Western blot analysis.

Transient transfection and reporter assay

MLO-Y4 cells were transfected with the indicated vectors by electroporation using a Microporator (Invitrogen, Carlsbad, CA) and Neon tips (Invitrogen) in accordance with the manufacturer's instructions. In each transfection, 0.25 μg of expression vector (NF-κB or pcDNA3.1), 0.2 μg of reporter and the *Renilla* luciferase plasmid were used as indicated. After 24 h, the cells were harvested, and luciferase activity was measured using the Dual-Glo luciferase assay kit (Promega, Madison, WI) according to the manufacturer's instructions. The relative luciferase activity was calculated after normalizing the transfection efficiency by *Renilla* luciferase activity.

Plasmid construction

The mouse *sost* promoter sequence (−2,072 to +11 bp) was selected for cloning by searching mouse genomic sequences (http://genome.ucsc.edu/). The *sost* promoter region was amplified by PCR using mouse genomic DNA as a template and subcloned into the *Kpn*I and *Mlu*I sites of pGL3b vector (Sost-WT-luc). Primers were obtained from MACROGEN (Seoul, Korea), and the primer sequences were as follows: *sost-Kpn*I 5'-GGT ACC CAC TCT CTG CTC GCT TGA TT-3′; *sost-Mlu*I 5′-GCG CAC GCG TGA AAG ACA CCT CCT CAG GTC-3′. To produce function-defective reporter constructs (Sost-MT1-luc, Sost-MT2-luc, or Sost-DM-luc) that contain mutations in the putative NF-κB binding site, site-directed mutagenesis PCR (GGGRNNYYC → GcGRNNYYC) was performed from −1,979 to −1,971 bp (MT1) and from −1,741 to −1,733 bp (MT2). The PCR primers used for the site-directed mutagenesis were as follows: MT1 forward (*f*) 5′-GAG TCC CCT TCC TGA GGG GAC TTC TGT CTG CC-3′, MT1 reverse (*r*) 5′-GGC AGA CAG AAG TCC CCT CAG GAA GGG GAC TC-3′, MT2 (*f*) 5′-GTC TTC CTC CAG GGC TGG GGA GTC CTC CAA CCT TC-3′, and MT2 (*r*) 5′-GAA GGT TGG AGG ACT CCC CAG CCC TGG AGG AAG AC-3′. The PCR products were digested with *Kpn*I and *Mlu*I, and the resulting fragments were ligated into pGL3b to produce the mutant reporters. Sost-DM-luc contains mutations in both sites. All constructs were verified by DNA sequencing.

Chromatin immunoprecipitation (ChIP)

The ChIP assay was performed as described previously (Cho et al., 2009). MLO-Y4 cells were cross-linked with 1% formaldehyde, lysed and sonicated to yield DNA fragments of approximately 200–800 bp. After preclearing with blocked protein G agarose, immunoprecipitation was performed with an anti-NF-κB antibody (Santa Cruz) or equivalent concentrations of normal rabbit IgG (Santa Cruz) as a negative control. DNA was eluted from immune complexes, purified and subjected to PCR amplification of the region containing the NF-κB binding element in the mouse *sost* promoter (−2,069 to −1,882 bp and −1,801 to −1,638 bp, respectively) using the following primer sets: primer 1 (*f*) 5′-GAT AGA TCA CCC CCA ACA AT-3′ and (*r*) 5′-CAT CTG TGG CGA TCT GCC TGG-3′ and primer 2 (*f*) 5′-TTA CCC AGT TAG CAT ACC ACA-3′ and (*r*) 5′-CAT GCC ACA GGG AGA AGG-3′, respectively.

Biotin pull-down assay

A biotin pull-down assay was conducted to analyze the in vitro binding of NF-κB to biotinylated DNA probes containing the NF-κB binding elements (probe 1: −1,989 to −1,961 bp, probe 2: −1,751 to −1,723 bp) in the mouse *sost* promoter. MLO-Y4 cells were transiently transfected with NF-κB expression plasmids and incubated for 24 h. Nuclear protein was isolated and incubated with 5′-biotinylated double-stranded DNA probes, followed by incubation with streptavidin–agarose beads. When indicated, non-biotinylated wild-type (WT) oligonucleotides or mutant (MT) oligonucleotides containing nucleotide substitutions in the NF-κB binding element were added to the reaction mixture in a 10-fold molar excess just prior to the addition of the biotinylated probe. The complex was pulled down, and proteins in the complex were analyzed by Western blotting with anti-NF-κB antibody. The DNA sequences of the oligonucleotides were as follows: probe 1 WT (f) 5′-CCC TTC CTG AGG GGA CTT CTG TCT GCC T-3′, probe 2

TABLE I. Primer Sequences for Quantitative RT-PCR

Genes	Forward	Reverse
Runx2	5′-TTCTCCAACCCACGA ATGCAC-3′	5′-CAGGTACGTGTGGTAGTGAGT-3′
Alp	5′-CCAACTCTTTTGTGCCAGAGA-3′	5′-GGCTACATTGGTGTTGAGCTTTT-3′
Ocn	5′-CTGACAAAGCCTTCATGTCCAA-3′	5′-GCGCCGGAGTCTGTTCACTA-3′
Rankl	5′-CAGCATCGCTCTGTTCCTGTA-3′	5′-CTGCGTTTTCATGGAGTCTCA-3′
Opg	5′-ACCCAGAAACTGGTCATCAGC-3′	5′-CTGCAATACACACACTCATCACT-3′
Sost	5′-AGCCTTCAGGAATGATGCCAC-3′	5′-CTTTGGCGTCATAGGGATGGT-3′
TNF-α	5′-GACGACAGCAAGGGACTAGC-3′	5′-GCTTTCTGTGCTCATGGTGC-3′
Gapdh	5′-TCACCATCTTCCAGGAGCG-3′	5′-CTGCTTACCACCTTCTTGA-3′

WT (f) 5′-CTC CAG GGC TGG GGA GTC CTC CAA CCT TC-3′, probe 1 MT (f) 5′-CCC TTC CTG AG**c** GGA CTT CTG TCT GCC T-3′ and probe 2 MT (f) 5′-CTC CAG GGC TG**c** GGA GTC CTC CAA CCT TC-3′.

Statistical analysis

The data are presented as the mean ± SD. The statistical significance of the results was assessed by Student's *t*-test. A *P*-value <0.05 was considered statistically significant.

Results

High-fat diet results in large increases in body weight and fat mass but decreases lean body mass

Over the course of the 12-week study, CON mice consumed 3.5 ± 0.70 g/day (13.6 ± 2.66 kcal/day) of the AIN-93M diet, and HF mice consumed 3.1 ± 0.93 g/day (16.3 ± 4.80 kcal/day). HF mice had higher body weights than CON mice from Week 4 of treatment until the end of the experiment (Fig. 1A). Over the 12-week experimental period, the body weight of the HF mice increased from 21.5 ± 1.4 g to 43.6 ± 4.0 g (+103.0%; $P < 0.01$ vs. Week 0 within group). The weight of the CON mice also increased from 21.5 ± 0.8 g to 32.9 ± 4.2 g (+52.8%; $P < 0.01$ vs. Week 0 within group). At the end of experiment, the total body fat mass determined by DEXA was 17.3 ± 3.5 g for the CON mice and 30.9 ± 3.3 g for the HF mice ($P < 0.0001$; Fig. 1B). However, the HF mice had lower lean body mass (9.6 ± 1.6 g) than that of CON mice (12.5 ± 1.8 g, $P < 0.01$; Fig. 1C).

High-fat diet decreases the cancellous vBMD and cortical bone thickness in femur

After 12 weeks on a high-fat diet, μCT measures revealed that HF mice had 17.0% lower cancellous vBMD (Th.BMD) in the distal femur compared to the CON mice (172 ± 32.3 vs. 207 ± 18.2 mg/cm^3, respectively; $P < 0.002$) (Fig. 2A,B). Significant decreases in the cancellous BV/TV and ConnD were also observed in the HF mice compared to the CON mice in the distal femur metaphysis (Fig. 2B). However, the Tb.Th, Tb.N, and Tb.Sp of the HF mice were not significantly different from those of the CON mice (Fig. 2B).

In the femoral midshaft, HF mice exhibited greater periosteal perimeter (T.Pm), reflecting periosteal expansion (Fig. 2C). However, the HF mice had a significantly greater medullary area (area inside the endocortical perimeter, M.Ar), and a smaller cortical shell thickness (Cs.Th). This periosteal expansion coupled with the increased marrow area in HF mice resulted in a reduced cross-sectional bone area (B.Ar) at the femoral midshaft (Fig. 2C), suggesting a net loss of cortical bone at this site. In spite of these changes, the pMOI of HF mice did not differ significantly from that of CON mice (Fig. 2C). There were no significant effects of the HF diet on the cortical vBMD at the distal or midshaft femur (data not shown).

High-fat diet decreases cancellous bone formation and increases bone resorption

After 12 weeks of the experimental period, HF mice had significantly lower cancellous bone volume than the CON mice. Histomorphometric analysis of undecalcified femur sections showed a threefold decrease in MAR in the HF mice compared to the CON mice (Fig. 3A,B). Although the MS/BS percentage was numerically reduced in HF mice compared to CON mice, this reduction did not reach statistical significance (Fig. 3B). These reductions in MAR and MS/BS contributed to the 73% reduction in the BFR of the HF mice (Fig. 3B). The percent osteoid surface in HF mice was 50% lower than in CON mice (Fig. 3B). Osteoid thickness tended to be lower in HF mice but it did not reach the statistical significance. The percent erosion surface increased sevenfold in HF mice compared to CON mice (Fig. 3B). These results suggest that high-fat diet reduces BMD by both reducing bone formation and enhancing bone resorption.

High-fat diet reduces the levels of osteogenic marker gene expression while increasing Rankl expression in tibial bone tissues

In an effort to decipher the mechanisms involved in low cancellous vBMD in HF mice, we further examined the expression levels of osteogenic and osteoclastogenic markers in tibial bone tissue. Runx2, osteocalcin (Ocn) and alkaline phosphatase (Alp) are well-known osteogenic marker genes. Real time-PCR analysis of tibial bone-derived RNA revealed that the expression levels of these osteogenic markers were lower in the HF mice than the CON mice, but statistical significance was only observed for Ocn expression (Fig. 4A). A significant increase in Rankl expression was observed in HF mice (vs. CON mice) (Fig. 4B). However, the expression level of osteoprotegerin (Opg) was the same in both groups, resulting in a dramatic increase in the Rankl:Opg ratio in the HF mice (Fig. 4B). These data suggest that high-fat diet-induced obesity decreases osteoblastic bone formation while upregulating osteoclastic bone resorption in limb bones.

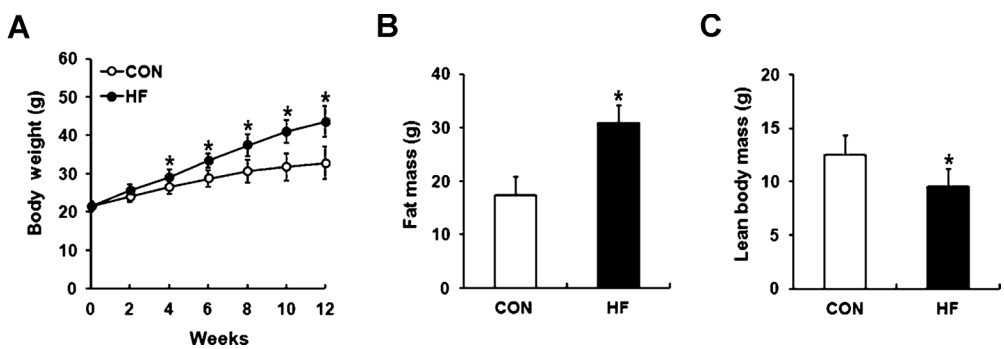

Fig. 1. The high-fat diet increased body weight and body fat mass while decreasing body lean mass. A: Body weights of the high-fat diet-fed (HF) or control diet-fed (CON) mice over 12 weeks. For both groups, n = 10. *Significant difference versus CON ($P < 0.01$). B, C: Total body fat mass and lean mass at Week 12 from whole body DEXA scans. *Significant difference versus CON ($P < 0.01$). Values are means ± SD.

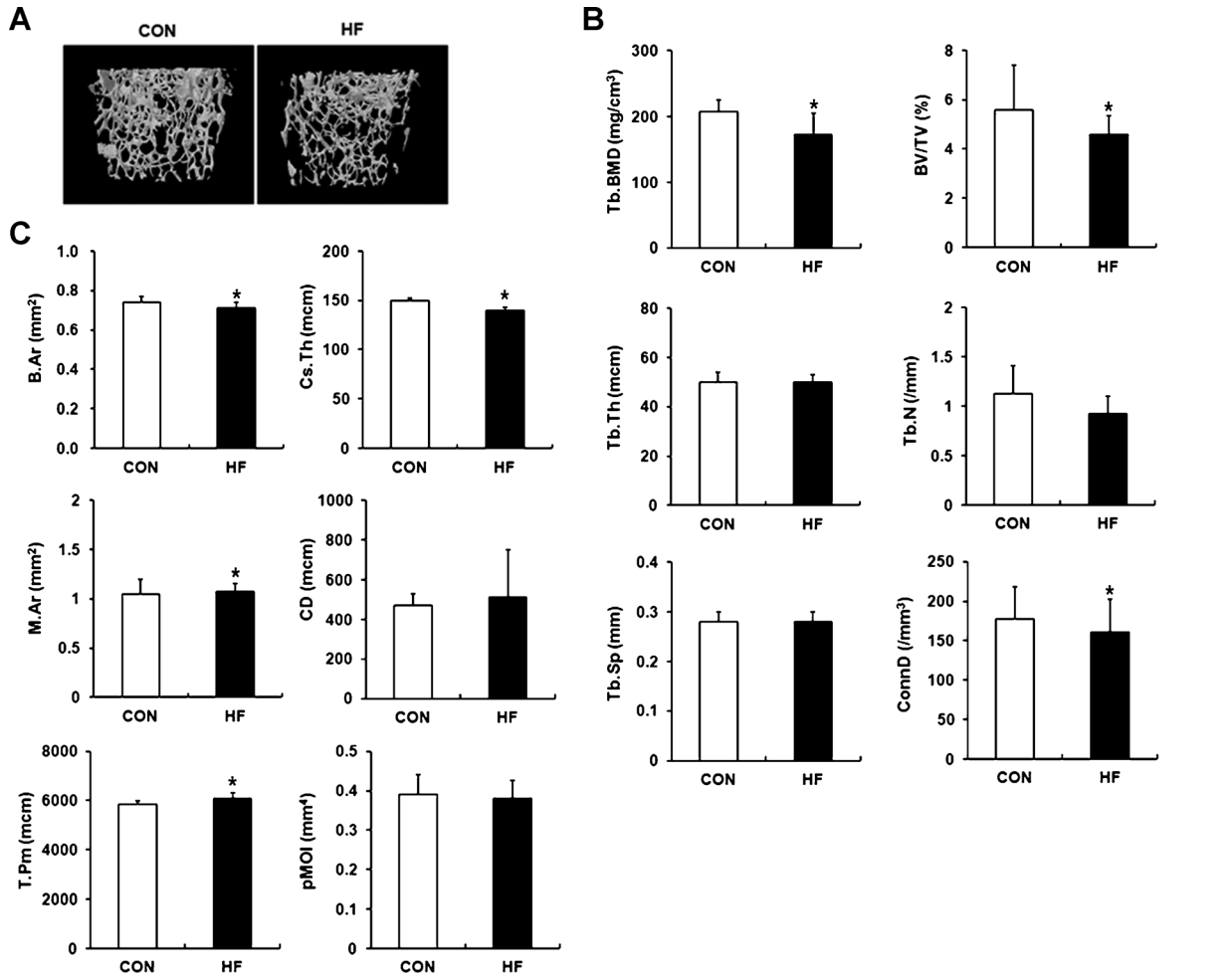

Fig. 2. The high-fat diet reduced the cancellous vBMD and the midshaft cortical bone thickness in the femur. A: Reconstituted three-dimensional μCT images of the distal femur cancellous bone from CON and HF mice. B: Ex vivo 3-dimensional μCT measures of distal femur cancellous bones from CON and HF mice. For both groups, n = 10. *$P < 0.05$ versus CON. Tb.BMD, trabecular vBMD; BV/TV, percent bone volume; Tb.Th, trabecular thickness; Tb.N, trabecular number; Tb.Sp, trabecular separation; ConnD, connectivity density. C: Ex vivo 2-dimensional μCT measures of the femur midshaft from CON and HF mice. For both groups, n = 10. *$P < 0.05$ versus CON. B.Ar, total cross-sectional bone area; Cs.Th, cortical thickness; M.Ar, medullary area; CD, cortical diameter; T.Pm, periosteal perimeter; pMOI, polar moment of inertia. Values are means ± SD.

High-fat diet increases TNF-α levels in serum and osteocytes

Because obesity is closely linked to the increased production of inflammatory cytokines such as TNF-α, we examined the TNF-α levels in the serum and bone tissue of HF mice. Immunohistochemical staining of TNF-α in femoral bone sections yielded a much stronger staining intensity in bone marrow cells and cortical osteocytes from HF mice compared to CON mice (Fig. 5A). An ELISA confirmed that the serum TNF-α level was 40% higher in the HF mice (Fig. 5B). Real time-PCR analysis of tibial bone-derived RNA was performed and an approximately sixfold increase in TNF-α mRNA was observed in HF mice compared to that of CON mice (Fig. 5C).

sost gene expression in the bone tissue increases in HF mice

We next examined the levels of in vivo sclerostin expression by immunohistochemical staining of femoral sections from CON and HF mice (Fig. 6A). There was no positive staining in the absence of primary antibody (data not shown). Compared to femur sections from CON mice, the overall sclerostin staining intensity in the osteocytes was much higher in the femoral sections from HF mice. We also employed real time-PCR to examine the levels of sclerostin mRNA in tibiae. As shown in Figure 6B, an approximately 20-fold increase in sclerostin transcripts was observed in HF mice compared to that of CON mice. These results indicate that high-fat diet-induced obesity results in increased sclerostin expression in bone tissues.

TNF-α enhances sclerostin expression in an NF-κB-dependent manner in MLO-Y4 cells

To elucidate the regulatory mechanism of obesity-induced sclerostin expression in our in vitro system, we examined the effect of TNF-α on sclerostin expression. MLO-Y4 cells were exposed to 10 ng/ml of TNF-α for lengths of time. TNF-α induced sclerostin expression but there was a fluctuation in sclerostin expression levels, as quantified by real time-PCR (Fig. 7A). Incubation for 2 h and 5 days showed significant increase in sclerostin mRNA levels. Next, we determined the

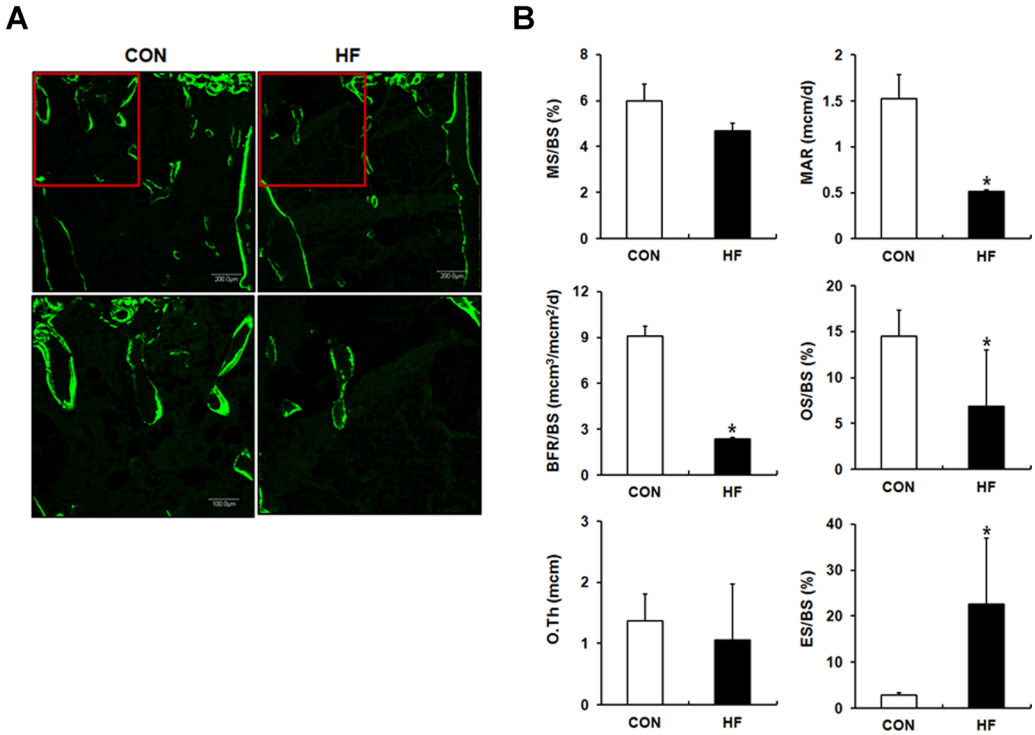

Fig. 3. The high-fat diet decreased cancellous bone formation but increased bone resorption. A: Representative sections of calcein-labeled distal femur of CON and HF mice. The lower panels are magnified images of the marked areas of their respective upper panels (upper panels: 100×, lower panels: 200×). B: Histomorphometric analysis results obtained from undecalcified distal femur sections of CON and HF mice. MAR, mineral apposition rate; MS/BS, percent mineralizing surface; BFR, bone formation rate; OS/BS, percent osteoid surface; O.Th, osteoid thickness; ES/BS, percent erosion surface. Values are means ± SD. For both groups, n = 10. *$P < 0.05$ versus CON.

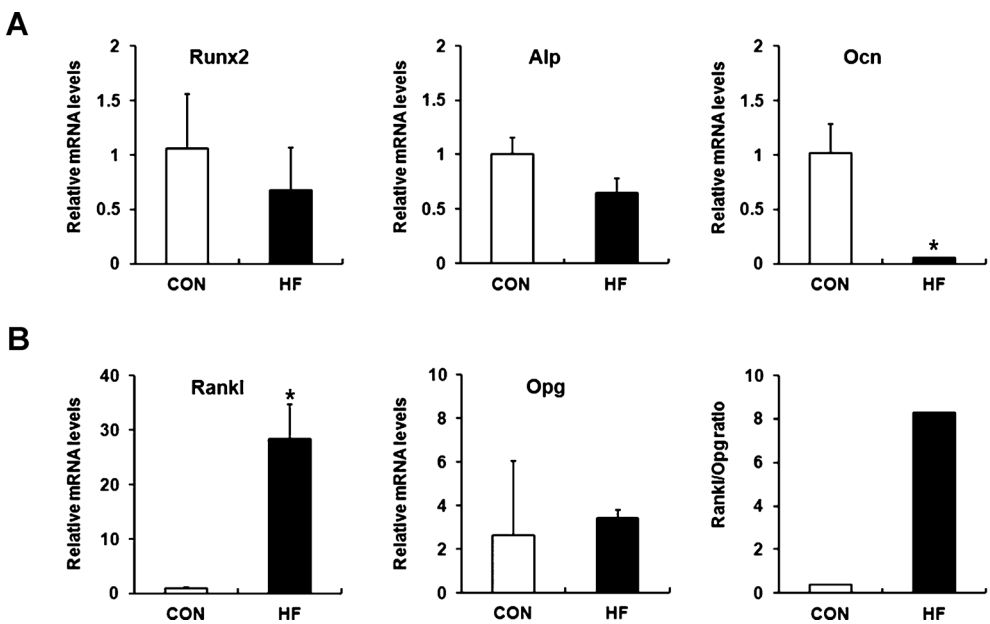

Fig. 4. The high-fat diet lowered the expression of osteogenic marker genes (A) while increasing the expression of osteoclastogenic genes (B). Real time-PCR analysis was performed with tibiae-derived RNA. The data represent the mean ± SD. *$P < 0.05$, compared to CON.

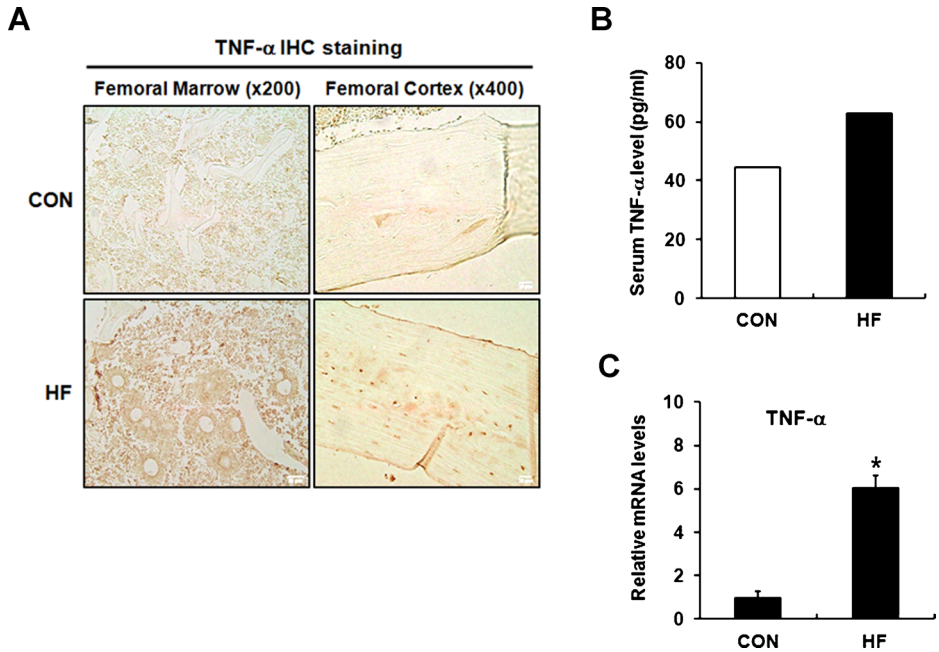

Fig. 5. The high-fat diet increased TNF-α levels in serum and bone tissues. A: Decalcified femoral sections were prepared from CON and HF mice and subjected to TNF-α immunohistochemical staining. The osteocytes and bone marrow cells from the HF mice showed a much stronger staining intensity compared to those from the CON mice. B: At sacrifice, serum was collected via cardiac puncture method, and the serum TNF-α levels were measured by a competitive ELISA assay. Data are presented as the mean of duplicates. C: Real time-PCR analysis of TNF-α was performed with tibiae-derived RNA. The data represent the mean ± SD of triplicates. *$P < 0.05$, compared to CON mice.

signaling pathway that was involved in TNF-α-induced sclerostin expression by treating cells with signal-specific inhibitors. MLO-Y4 cells were treated with TNF-α in the presence or absence of an ERK inhibitor (U0126), a JNK inhibitor (SP600125), a p38 MAPK inhibitor (SB203580) or an NF-κB inhibitor (BAY-11-7082). Real-time PCR and Western blot analysis demonstrated that TNF-α-induced sclerostin expression was blocked by the inhibition of NF-κB activation, but not by inhibiting JNK, ERK or p38 MAPK activation (Fig. 7B,C).

To further investigate the NF-κB-dependent regulatory mechanism of sclerostin expression, we examined whether NF-κB (p65) overexpression increase sclerostin expression. Increase in sclerostin expression in NF-κB transfected cells was confirmed by real-time PCR and Western blot analysis (Fig. 8A,B). To further verify the role of NF-κB in sclerostin expression, we knocked down the expression of NF-κB (p65) in MLO-Y4 cells using siRNA. Knockdown efficiency of NF-κB siRNA was confirmed by Western blot analysis. The knockdown of NF-κB significantly decreased TNF-α-induced sclerostin expression (Fig. 8C). These results indicate that TNF-α-induced sclerostin expression requires the activation of the NF-κB signaling pathway.

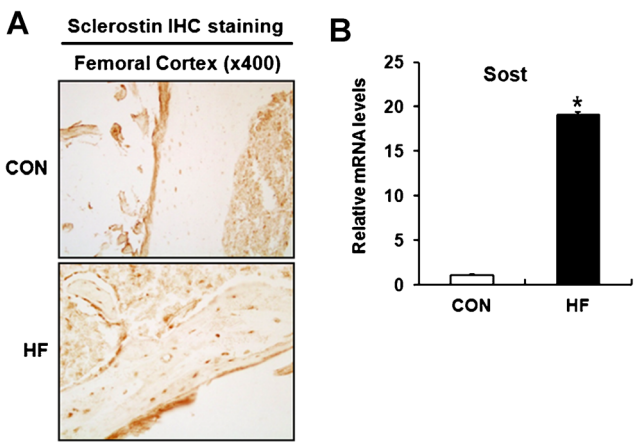

Fig. 6. The high-fat diet increased sclerostin expression in bone tissues. A: Immunohistochemical staining for sclerostin was performed on decalcified femoral sections from CON and HF mice. The number of osteocytes positive for sclerostin in the femoral cortex was much higher in HF mice than in CON mice. B: Real time-PCR analysis was performed with tibiae-derived RNA. The data represent the mean ± SD of triplicates. *$P < 0.05$, compared to CON.

NF-κB directly binds to the sost promoter and stimulates sclerostin transcription

To investigate whether NF-κB directly regulates sclerostin expression, we performed an in silico analysis to search for the NF-κB binding element (GGGRNNYYC) in the mouse *sost* promoter using the Transcription Element Search System and found two putative NF-κB binding elements at −1,979 to −1,971 bp and −1,741 to −1,733 bp within the ~2.2 kb mouse *sost* promoter region (Fig. 9A). To examine whether NF-κB binds to these putative NF-κB binding motifs in vivo, we performed ChIP. MLO-Y4 cells were treated with 50 ng/ml of TNF-α for 24 h, and DNA fragments were immunoprecipitated with an anti-NF-κB antibody or control IgG. PCR amplification

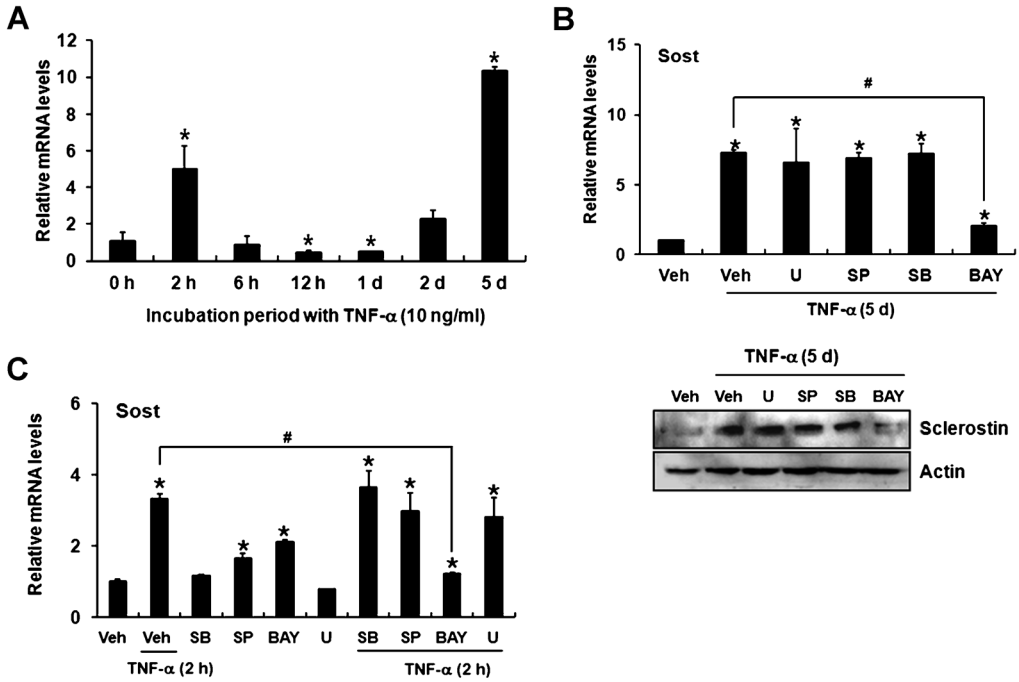

Fig. 7. TNF-α induced the expression of sclerostin in MLO-Y4 cells. MLO-Y4 cells were incubated with TNF-α (10 ng/ml) for the indicated periods of time (A) or incubated with TNF-α (10 ng/ml) for 2 h or 5 days in the presence or absence of an ERK inhibitor (U0126, U), a JNK inhibitor (SP600125, SP), a p38 MAPK inhibitor (SB203580, SB) or an NF-κB inhibitor (BAY-11-7082, BAY) (B, C). Sclerostin mRNA or protein levels were then analyzed by real time-PCR (A, B, C upper panel) and Western blot analysis (C lower panel), respectively. The relative sclerostin mRNA level was normalized to Gapdh. The data represent the mean ± SD of triplicates. *$P < 0.05$ versus 0 h (A) or Veh only (B, C), #$P < 0.05$.

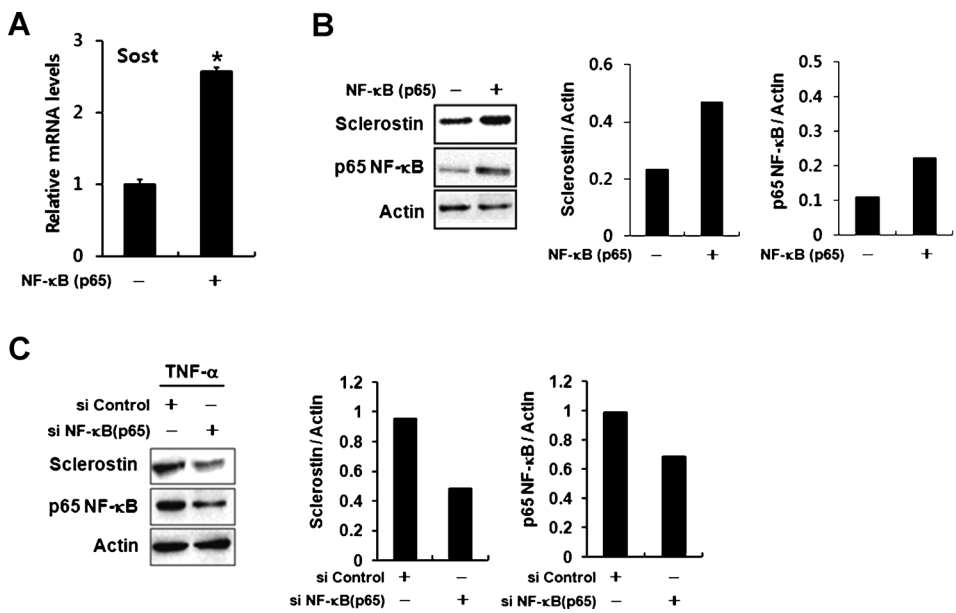

Fig. 8. TNF-α enhanced sclerostin expression in an NF-κB-dependent manner in MLO-Y4 cells. A, B: MLO-Y4 cells were transiently transfected with the pcDNA or NF-κB p65 expression vector and incubated for 24 h. Real time-PCR (A) and Western blot analysis (B) were then performed. The real time-PCR data were represented as the mean ± SD of triplicates (*$P < 0.05$). C: MLO-Y4 cells were transfected with siRNA for NF-κB p65 or nontargeting control siRNA. The effect of NF-κB p65 knockdown on the expression of sclerostin was analyzed by Western blot analysis. For Western blot data, densitometric analysis for band intensity was performed and the results were shown as the relative ratio to Actin band intensity (B, C).

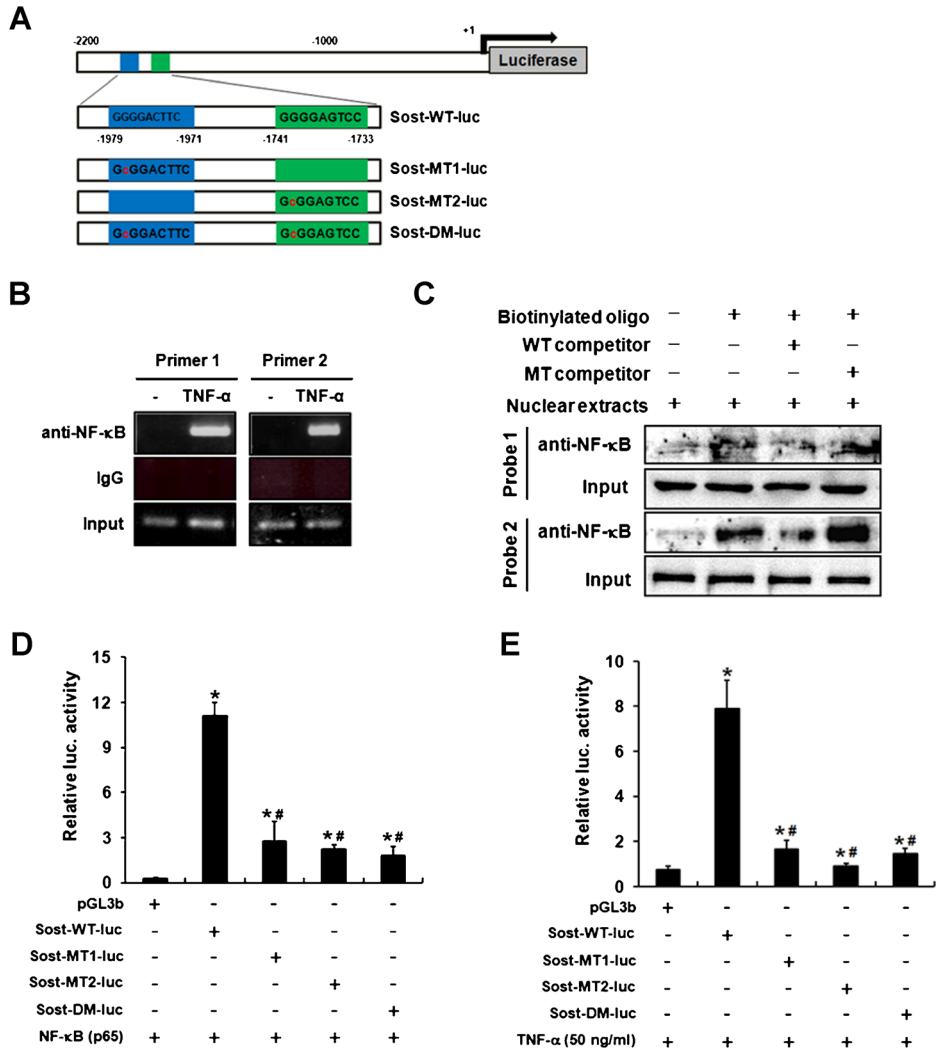

Fig. 9. NF-κB bound directly to the sost promoter and stimulates sclerostin transcription. A: Schematic illustration of the luciferase reporter containing the mouse *sost* promoter. The highlighted bars show the nucleotide sequence of the mouse *sost* promoter regions that contain the NF-κB binding element (GGGRNNYYC). The mutant reporters include nucleotide substitutions in the NF-κB binding element (GGGRNNYYC → GcGRNNYYC) in one or both of the binding elements. B: MLO-Y4 cells were treated with TNF-α (10 ng/ml) for 5 days, and cellular DNA fragments were immunoprecipitated with an anti-NF-κB antibody or normal IgG. PCR amplification revealed that NF-κB binds to the genomic DNA region encompassing the NF-κB binding elements (primer 1: 1,979 to 1,971 bp, primer 2: 1,741 to 1,733 bp) on the *sost* promoter. (C) Nuclear proteins were prepared from NF-κB overexpressing cells and incubated with 5′-biotinylated double stranded oligonucleotides that contain the NF-κB binding element. When indicated, nonbiotinylated wild-type oligonucleotides (WT competitor) or mutant oligonucleotides (MT competitor) were added to the reaction mixture in a 10-fold excess. The mutant competitor includes nucleotide substitutions in NF-κB binding element (probe 1: GG GGA CTT C → Gc GGA CTT C, probe 2: GG GGA GTC C → Gc GGA GTC C). Biotinylated DNA-protein complexes were then pulled down with streptavidin-agarose beads and bound NF-κB was detected by immunoblotting with anti-NF-κB antibody. D, E: MLO-Y4 cells were transfected with p65 NF-κB expression plasmids (C) or treated with 50 ng/ml of TNF-α (D) and incubated for 24 h, and then, luciferase activity was measured. The data are shown as activity relative to *Renilla* luciferase activity and represent the mean ± SD (N = 6, *$P < 0.05$ vs. pGL3b, #$P < 0.05$ vs. Sost-WT-luc).

of the *sost* promoter regions containing each of the two putative NF-κB binding elements revealed that NF-κB binds to both DNA regions encompassing the putative binding elements (Fig. 9B). PCR amplification of the DNA fragments immunoprecipitated with control IgG did not produce any amplified DNA bands, suggesting that the PCR reactions are specific.

To further verify the direct binding of NF-κB to the *sost* promoter in vitro, we conducted a biotin pull-down assay. Nuclear proteins were isolated from NF-κB overexpressing cells and incubated with biotinylated double-stranded oligonucleotides whose sequence was composed of −1,989 to −1,961 bp (probe 1) and −1,751 to −1,723 bp (probe 2) of the mouse *sost* gene promoter. The complex was pulled down with streptavidin–agarose beads, and the eluted proteins were subjected to Western blot analysis with the anti-NF-κB antibody. Consistent with the ChIP assay results, NF-κB bound to the oligonucleotides containing the NF-κB binding motif in the *sost* promoter in vitro (Fig. 9C). When nonbiotinylated oligonucleotides were added to the reaction mixture in a 10-fold excess, NF-κB binding to biotinylated probes was abolished by WT oligonucleotides but not by MT oligonucleotides in which one nucleotide within the NF-κB binding motif were substituted. These results further suggest

that NF-κB directly binds to the *sost* promoter in a sequence-specific manner.

We then used a luciferase reporter assay to examine whether NF-κB overexpression or TNF-α treatment transactivates the *sost* promoter (Fig. 9D,E). Overexpression of p65 NF-κB significantly increased the reporter activity of Sost-WT-luc, which contains the 2.2 kb mouse *sost* promoter sequence (Fig. 9D). Mutations in either of the NF-κB binding elements suppressed reporter activity, but mutations in both elements did not further suppress the reporter activity (Fig. 9D). Treatment of cells with 50 ng/ml of TNF-α for 24 h significantly enhanced Sost-WT-luc reporter activity (Fig. 9E). Similar to the responses to NF-κB overexpression, mutations in either of the NF-κB binding elements suppressed TNF-α-induced reporter activity (Fig. 9E). Taken together, these results indicate that NF-κB binds directly to the *sost* promoter, thus inducing the transcription of the *sost* gene.

Discussion

This experiment is the first to examine sclerostin expression in the context of a high-fat diet-induced obesity in growing mice. The mechanism by which TNF-α regulates sclerostin expression was also elucidated in this study.

Our primary hypotheses were that (1) high-fat diet-induced obesity would lead to the enhanced sclerostin expression and (2) TNF-α, which is increased in obesity, would be involved in the obesity-induced sclerostin expression in bone tissues. Our results are consistent with these working hypotheses and suggest that high-fat diet-induced obesity reduces bone mass partially via TNF-α-induced sclerostin expression.

In the present study, the high-fat diet resulted in significant decreases in the cancellous vBMD and reduced the architectural quality in the femur. Mounting evidence shows the effects of a high-fat diet (or high-fat diet-induced obesity) on bone mass and quality. Parhami et al. (2001) showed that the femoral mineral content of C57BL/6 mice on a high-fat diet was 43% lower, and the mineral density was 15% lower than that of mice fed the chow diet. Ocn expression was also reduced in the marrow of the C57BL/6 mice fed the high-fat diet. Others have shown that both young and adult mice fed a high-fat diet displayed dramatically lower femoral strength, stiffness and toughness than control animals (Ionova-Martin et al., 2011). A reduced structural quality denoted by the inferior lamellar and osteocyte alignment was also demonstrated in both age groups. Significant negative correlations between body composition, adiponectin and bone parameters were reported, demonstrating that a high-fat diet consumed during the growing period has deleterious effects on bone integrity parameters in mice (Lac et al., 2008). However, to our knowledge, no study has demonstrated the molecular mechanism of bone loss in the context of obesity which links increased levels of TNF-α and sclerostin expression in bone tissues.

To determine whether the loss of cancellous vBMD that resulted from the high-fat diet was caused by increased resorption and/or decreased bone formation, we examined histomorphometric measurements of these variables. A dramatic increase in the bone resorbing surface was observed in the HF mice. Regulation of osteoclast number or activity by a high-fat diet could be mediated by the regulation of Rankl/Opg expression. Previously reports demonstrated that the Rankl/Opg expression ratio is increased in T-lymphocytes and bone marrow stromal/osteoblastic cells isolated from the bone marrow of the high-fat group (Cao et al., 2009; Graham et al., 2010). Consistent with this observation, we found an increase in Rankl expression in HF mice (vs. CON mice). The expression level of Opg was not different between the two groups. The Rankl/Opg ratio thus increased in the HF mice compared to CON mice, supporting the histomorphometric observation of a dramatic increase in the bone resorbing surface in HF mice. Because TNF-α is a strong inducer of Rankl expression, increased TNF-α expression in bone marrow cells and osteocytes may partially contribute to the enhanced Rankl expression in HF mice.

In the context of bone formation, the large decreases in the MAR and percent mineralizing surface contributed to the nearly 73% reduction in the BFR in the mice fed a high-fat diet. The reduced BFR was due more to a reduced MAR rather than to changes in the % MS/BS, suggesting that declined osteoblast activity rather than declined osteoblast recruitment was responsible for the reduced BFR with high-fat diet. Another indicator of osteoblast activity, percent osteoid surface, was also reduced by the high-fat diet. In accordance with these data, high-fat diet-induced obesity decreased the expression of Ocn in bone tissue. Furthermore, these osteogenic histomorphometric assessment values were inversely associated with the sclerostin expression level in bone tissue. The high-fat diet-induced reduction in bone density has been previously shown to be associated with the suppression of β-catenin expression in growing mice (Chen et al., 2010). Together with this report, our results provide evidence supporting the hypothesis that compromised bone formation observed in high-fat diet fed growing mice is associated with increased sclerostin expression. Therefore, it is assumed that highly expressed sclerostin in the context of high-fat diet would antagonize Wnt/β-catenin signaling in the long bones, contributing to a high-fat diet-induced bone loss.

Our results demonstrate that sclerostin is a novel target of TNF-α-activated NF-κB and this observation could explain how TNF-α cooperates with sclerostin to suppress bone formation in the context of high-fat diet-induced obesity. The data presented in this study supports this hypothesis: First, ChIP assay results showed that TNF-α–activated NF-κB binds to the NF-κB binding element on the *sost* promoter in vivo. Second, biotin pull-down assay demonstrated that NF-κB binds to 5′ biotinylated double-stranded oligonucleotides that contain the NF-κB binding element in vitro. Third, TNF-α stimulates *sost* promoter activity in an NF-κB binding element-dependent manner. Fourth, overexpression and knockdown of NF-κB substantially increased and decreased the expression levels of sclerostin, respectively. These results of our study indicate that NF-κB directly binds to and transactivates the *sost* promoter, thus increasing sclerostin expression. Histological analysis demonstrated that HF mice expressed higher levels of TNF-α and sclerostin protein in bone tissues and especially in osteocytes. Others have reported that TNF-related weak inducer of apoptosis (TWEAK) and TNF-α induce sclerostin expression in human osteoblasts (Vincent et al., 2009). In addition, a recent report showed that TNF-α mediates the sclerostin expression in ovariectomized mice (Kim et al., 2012). Therefore, it is suggested that in various conditions that induce TNF-α expression, including obesity and estrogen deficiency, TNF-α contributes to bone loss partially by inducing sclerostin expression in bone. Notwithstanding the results demonstrated in the present study, the underlying mechanism how increased level of TNF-α relates to the obesity-induced bone loss has not been fully investigated as of now. Mounting evidence shows that relevance of TNF-α to the inflammatory condition (e.g., rheumatoid arthritis, diabetes) induced bone loss (Saidenberg-Kermanac'h et al., 2004; Coe et al., 2011; Roux, 2011). To better support of direct involvement of TNF-α in obesity and sclerostin expression, future studies with using (1) TNF-α-null background mice fed with control and HF diet or (2) HF diet fed mice treated with anti-TNF-α antibodies are justified. A higher body mass confers a higher mechanical load on to the skeletal muscles and bone. The resulting increased muscle mass and strength may provide beneficial effect to the bone and counterbalance the

biochemical changes that induce bone loss in obese individuals. Classically, it has been thought that obese children and adults have increased lean mass as well as fat mass (Forbes and Welle, 1983). However, in the present study, the lean body mass was found to be significantly lower in HF mice than CON mice. In light of recent studies showing the effect of body fat on skeletal muscle mass, diet-induced obesity appears to interfere with muscle development. Insulin plays a critical role in muscle protein synthesis by activating the downstream targets of mTOR (Kimball et al., 1998; Balage et al., 2001; Prod'homme et al., 2005). There is mounting evidence that the Akt/mTOR pathway is dysregulated in animal models of diet-induced obesity (Eldar-Finkelman et al., 1999) and in human studies of fatty acid infusion (Belfort et al., 2005). In addition, it has been reported that a chronic high-fat diet impairs the ability of skeletal muscle to grow in response to mechanical load in growing mice, and this impairment coincides with a failure to activate the Akt/mTOR signaling pathway (Sitnick et al., 2009). Therefore, considering these reports and our data, the main effect of high-fat diet-induced obesity on limb bones is likely to be a negative regulation of bone rather than mechanical load-induced bone gain.

In summary, growing mice fed a high-fat diet over 12 weeks exhibited significant bone loss in their femurs and increased TNF-α and sclerostin expression in ostecytes. The high-fat diet reduced bone mass by decreasing bone formation and increasing bone resorption. The data presented in this study demonstrated that TNF-α is a transcriptional activator for sclerostin. The findings from the present study support a model in which, in the context of obesity or other inflammatory disease increasing production of TNF-α, TNF-α enhances bone loss via the induction of sclerostin expression in an NF-κB-dependent manner.

Literature Cited

Bacchetta J, Boutroy S, Guebre-Egziabher F, Juillard L, Drai J, Pelletier S, Richard M, Charrie A, Carlier MC, Chapurlat R, Laville M, Fouque D. 2009. The relationship between adipokines, osteocalcin and bone quality in chronic kidney disease. Nephrol Dial Transplant 24:3120–3125.

Baek K, Bloomfield SA. 2009. Beta-adrenergic blockade and leptin replacement effectively mitigate disuse bone loss. J Bone Miner Res 24:792–799.

Baek K, Bloomfield SA. 2012. Blocking beta-adrenergic signaling attenuates reductions in circulating leptin, cancellous bone mass, and marrow adiposity seen with dietary energy restriction. J Appl Physiol 113:1792–1801.

Balage M, Sinaud S, Prod'homme M, Dardevet D, Vary TC, Kimball SR, Jefferson LS, Grizard J. 2001. Amino acids and insulin are both required to regulate assembly of the eIF4E. eIF4G complex in rat skeletal muscle. Am J Physiol Endocrinol Metab 281:E565–E574.

Belfort R, Mandarino L, Kashyap S, Wirfel K, Pratipanawatr T, Berria R, Defronzo RA, Cusi K. 2005. Dose-response effect of elevated plasma free fatty acid on insulin signaling. Diabetes 54:1640–1648.

Bozic B, Loncar G, Prodanovic N, Radojicic Z, Cvorovic V, Dimkovic S, Popovic-Brkic V. 2010. Relationship between high circulating adiponectin with bone mineral density and bone metabolism in elderly males with chronic heart failure. J Card Fail 16:301–307.

Brunkow ME, Gardner JC, Van Ness J, Paeper BW, Kovacevich BR, Proll S, Skonier JE, Zhao L, Sabo PJ, Fu Y, Alisch RS, Gillett L, Colbert T, Tacconi P, Galas D, Hamersma H, Beighton P, Mulligan J., 2001. Bone dysplasia sclerosteosis results from loss of the SOST gene product, a novel cystine knot-containing protein. Am J Hum Genet 68:577–589.

Cao JJ, Gregoire BR, Gao H., 2009. High-fat diet decreases cancellous bone mass but has no effect on cortical bone mass in the tibia in mice. Bone 44:1097–1104.

Chan G, Chen CT. 2009. Musculoskeletal effects of obesity. Curr Opin Pediatr 21:65–70.

Chen JR, Lazarenko OP, Wu X, Tong Y, Blackburn ML, Shankar K, Badger TM, Ronis MJ. 2010. Obesity reduces bone density associated with activation of PPARgamma and suppression of Wnt/beta-catenin in rapidly growing male rats. PLoS ONE 5:e13704.

Cho YD, Yoon WJ, Woo KM, Baek JH, Lee G, Cho JY, Ryoo HM. 2009. Molecular regulation of matrix extracellular phosphoglycoprotein expression by bone morphogenetic protein-2. J Biol Chem 284:25230–25240.

Coe LM, Irwin R, Lippner D, McCabe LR. 2011. The bone marrow microenvironment contributes to type I diabetes induced osteoblast death. J Cell Physiol 226:477–483.

Cope AP, Liblau RS, Yang XD, Congia M, Laudanna C, Schreiber RD, Probert L, Kollias G, McDevitt HO. 1997. Chronic tumor necrosis factor alters T cell responses by attenuating T cell receptor signaling. J Exp Med 185:1573–1584.

Dempster DW, Compston JE, Drezner MK, Glorieux FH, Kanis JA, Malluche H, Meunier PJ, Ott SM, Recker RR, Parfitt AM. 2013. Standardized nomenclature, symbols, and units for bone histomorphometry: A 2012 update of the report of the ASBMR Histomorphometry Nomenclature Committee. J Bone Miner Res 28:2–17.

Eldar-Finkelman H, Schreyer SA, Shinohara MM, LeBoeuf RC, Krebs EG. 1999. Increased glycogen synthase kinase-3 activity in diabetes- and obesity-prone C57BL/6J mice. Diabetes 48:1662–1666.

Forbes GB, Welle SL., 1983. Lean body mass in obesity. Int J Obes 7:99–107.

Graham LS, Tintut Y, Parhami F, Kitchen CM, Ivanov Y, Tetradis S, Effros RB. 2010. Bone density and hyperlipidemia: The T-lymphocyte connection. J Bone Miner Res 25:2460–2469.

Hotamisligil GS., 2006. Inflammation and metabolic disorders. Nature 444:860–867.

Hsu SM, Raine L, Fanger H. 1981. Use of avidin-biotin-peroxidase complex (ABC) in immunoperoxidase techniques: A comparison between ABC and unlabeled antibody (PAP) procedures. J Histochem Cytochem 29:577–580.

Ionova-Martin SS, Wade JM, Tang S, Shahnazari M, Ager JW III, Lane NE, Yao W, Alliston T, Vaisse C, Ritchie RO. 2011. Changes in cortical bone response to high-fat diet from adolescence to adulthood in mice. Osteoporos Int 22:2283–2293.

Kim BJ, Bae SJ, Lee SY, Lee YS, Baek JE, Park SY, Lee SH, Koh JM, Kim GS. 2012. TNF-alpha mediates the stimulation of sclerostin expression in an estrogen-deficient condition. Biochem Biophys Res Commun 424:170–175.

Kimball SR, Horetsky RL, Jefferson LS. 1998. Signal transduction pathways involved in the regulation of protein synthesis by insulin in L6 myoblasts. Am J Physiol 274: C221–C228.

Lac G, Cavalie H, Ebal E, Michaux O. 2008. Effects of a high fat diet on bone of growing rats. Correlations between visceral fat, adiponectin and bone mass density. Lipids Health Dis 7:16.

Lee HL, Yi T, Woo KM, Ryoo HM, Kim GS, Baek JH. 2010. Msx2 mediates the inhibitory action of TNF-alpha on osteoblast differentiation. Exp Mol Med 42:437–445.

Li X, Ominsky MS, Niu QT, Sun N, Daugherty B, D'Agostin D, Kurahara C, Gao Y, Cao J, Gong J, Asuncion F, Barrero M, Warmington K, Dwyer D, Stolina M, Morony S, Sarosi I, Kostenuik PJ, Lacey DL, Simonet WS, Ke HZ, Paszty C. 2008. Targeted deletion of the sclerostin gene in mice results in increased bone formation and bone strength. J Bone Miner Res 23:860–869.

McMahon MS, Ueki Y., 2008. Does anti-TNF-alpha have a role in the treatment of osteoporosis? Bull NYU Hosp Jt Dis 66:280–281.

Parfitt AM, Drezner MK, Glorieux FH, Kanis JA, Malluche H, Meunier PJ, Ott SM, Recker RR. 1987. Bone histomorphometry: Standardization of nomenclature, symbols, and units. Report of the ASBMR Histomorphometry Nomenclature Committee. J Bone Miner Res 2:595–610.

Parhami F, Tintut Y, Beamer WG, Gharavi N, Goodman W, Demer LL. 2001. Atherogenic high-fat diet reduces bone mineralization in mice. J Bone Miner Res 16:182–188.

Prod'homme M, Balage M, Debras E, Farges MC, Kimball S, Jefferson L, Grizard J. 2005. Differential effects of insulin and dietary amino acids on muscle protein synthesis in adult and old rats. J Physiol 563:235–248.

Reeves PG, Nielsen FH, Fahey GC, Jr. 1993a. AIN-93 purified diets for laboratory rodents: Final report of the American Institute of Nutrition ad hoc writing committee on the reformulation of the AIN-76A rodent diet. J Nutr 123:1939–1951.

Reeves PG, Rossow KL, Lindlauf J. 1993b. Development and testing of the AIN-93 purified diets for rodents: Results on growth, kidney calcification and bone mineralization in rats and mice. J Nutr 123:1923–1931.

Roux C. 2011. Anti-TNFα therapy and prevention of bone loss in rheumatoid arthritis. IBMS BoneKEy 8:154–158.

Saidenberg-Kermanac'h N, Corrado A, Lemeiter D, deVernejoul MC, Boissier MC, Cohen-Solal ME. 2004. TNF-alpha antibodies and osteoprotegerin decrease systemic bone loss associated with inflammation through distinct mechanisms in collagen-induced arthritis. Bone 35:1200–1207.

Sitnick M, Bodine SC, Rutledge JC. 2009. Chronic high fat feeding attenuates load-induced hypertrophy in mice. J Physiol 587:5753–5765.

Takeda S, Elefteriou F, Levasseur R, Liu X, Zhao L, Parker KL, Armstrong D, Ducy P, Karsenty G. 2002. Leptin regulates bone formation via the sympathetic nervous system. Cell 111:305–317.

Urano T, Shiraki M, Ouchi Y, Inoue S. 2012. Association of circulating sclerostin levels with fat mass and metabolic disease-related markers in Japanese postmenopausal women. J Clin Endocrinol Metab 97:E1473–E1477.

Vincent C, Findlay DM, Welldon KJ, Wijenayaka AR, Zheng TS, Haynes DR, Fazzalari NL, Evdokiou A, Atkins GJ. 2009. Pro-inflammatory cytokines TNF-related weak inducer of apoptosis (TWEAK) and TNFalpha induce the mitogen-activated protein kinase (MAPK)-dependent expression of sclerostin in human osteoblasts. J Bone Miner Res 24:1434–1449.

Xiao Y, Cui J, Shi YH, Sun J, Wang ZP, Le GW. 2010. Effects of duodenal redox status on calcium absorption and related genes expression in high-fat diet-fed mice. Nutrition 26:1188–1194.

Zhang YH, Heulsmann A, Tondravi MM, Mukherjee A, Abu-Amer Y. 2001. Tumor necrosis factor-alpha (TNF) stimulates RANKL-induced osteoclastogenesis via coupling of TNF type 1 receptor and RANK signaling pathways. J Biol Chem 276:563–568.

Zhao LJ, Liu YJ, Liu PY, Hamilton J, Recker RR, Deng HW. 2007. Relationship of obesity with osteoporosis. J Clin Endocrinol Metab 92:1640–1646.

Zhao LJ, Jiang H, Papasian CJ, Maulik D, Drees B, Hamilton J, Deng HW. 2008. Correlation of obesity and osteoporosis: Effect of fat mass on the determination of osteoporosis. J Bone Miner Res 23:17–29.